AD-A080 225 NATIONAL BUREAU OF STANDARDS WASHINGTON DC FRACTURE A--ETC F/G 11/2
STRESS CORROSION OF CERAMIC MATERIALS.(U)
DEC 79 S W FREIMAN, S M WIEDERHORN N00014-79-F-0030

UNCLASSIFIED NL

1 OF 1
AD A080225

END
DATE FILMED
3-80
DDC

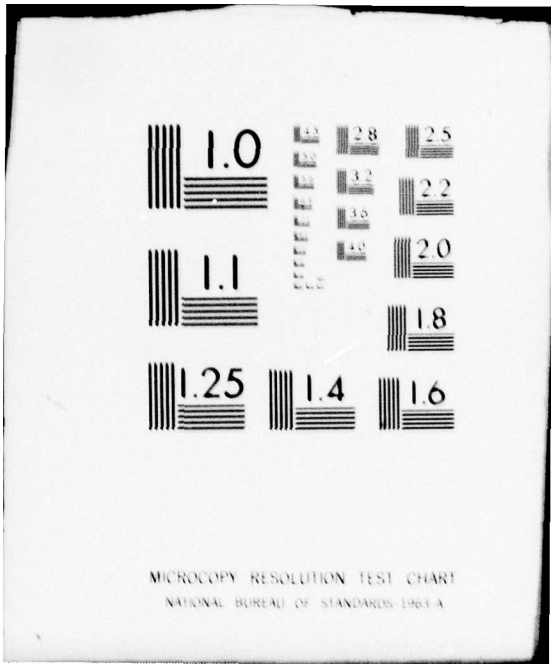
1.0
1.1
1.25
1.4
1.6
2.8
3.2
3.6
2.5
2.2
2.0
1.8
MICROCOPY RESOLUTION TEST CHART
NATIONAL BUREAU OF STANDARDS 1963-A

(12)

Stress Corrosion of Ceramic Materials

S. W. Freiman, et al

Technical Report

ONR Contract No. N00014-79F-0030
NBS Project No. 5620454

For

Office of Naval Research
Arlington, VA. 22217

By

National Bureau of Standards
Washington, D. C. 20234

December 1979

Unclassified

SECURITY CLASSIFICATION OF THIS PAGE (When Data Entered)

REPORT DOCUMENTATION PAGE

READ INSTRUCTIONS BEFORE COMPLETING FORM

1. REPORT NUMBER

2. GOVT ACCESSION NO.

3. RECIPIENT'S CATALOG NUMBER

4. TITLE (and Subtitle)
Stress Corrosion of Ceramic Materials

5. TYPE OF REPORT & PERIOD COVERED
Annual rept.
1 Mar [redacted] — 30 Sep [redacted] 79

6. PERFORMING ORG. REPORT NUMBER

7. AUTHOR(s)
S. W. Freiman, S. M. Wiederhorn, C. J. Simmons, E. R. Fuller, Jr., P. N. Krishnan, G. E. Walrafen, D. M. Sanders

8. CONTRACT OR GRANT NUMBER(s)
N0014-79-F-0030

9. PERFORMING ORGANIZATION NAME AND ADDRESS
National Bureau of Standards
Fracture and Deformation Division
Washington, D. C. 20234

10. PROGRAM ELEMENT, PROJECT, TASK AREA & WORK UNIT NUMBERS
61153N, RR 022-02-01 (471)

11. CONTROLLING OFFICE NAME AND ADDRESS
Office of Naval Research
800 North Quincy
Arlington, VA. 22217

12. REPORT DATE
1 Dec [redacted] 79

13. NUMBER OF PAGES
41

14. MONITORING AGENCY NAME & ADDRESS (if different from Controlling Office)
RR02202
RR022020 1

15. SECURITY CLASS. (of this report)
Unclassified

15a. DECLASSIFICATION/DOWNGRADING SCHEDULE

16. DISTRIBUTION STATEMENT (of this Report)

17. DISTRIBUTION STATEMENT (of the abstract entered in Block 20, if different from Report)

18. SUPPLEMENTARY NOTES

19. KEY WORDS (Continue on reverse side if necessary and identify by block number)

Crack growth	Surface analysis
Stress corrosion	ESCA
Glasses	Raman Spectroscopy
Ceramics	Proof testing

20. ABSTRACT (Continue on reverse side if necessary and identify by block number)

A film deposition and surface analysis system has been set up. This system will be used for the analysis of the effect of stress on chemical reactions of ceramics with environments such as water. Preliminary results of Raman spectroscopy experiments suggest that there is an increase in the number of defects in the structure of fused silica under stress. A model describing the effect of water diffusion controlled crack growth has been derived. It was shown that the presence of a relatively K_0 independent region of crack growth has a significant effect on proof testing.

DD FORM 1 JAN 73 1473 EDITION OF 1 NOV 65 IS OBSOLETE
S/N 0102-LF-014-6601

SECURITY CLASSIFICATION OF THIS PAGE (When Data Entered)

411561

FOREWORD

This report describes the results of an experimental program to investigate mechanisms of stress corrosion in ceramics and to determine the effect of this phenomenon on fracture. Progress toward these goals is summarized in the following sections.

TABLE OF CONTENTS

RE: Contract N00014-79-F-0030
Contract number is valid. It is a delivery order number

INTRODUCTION

One of the main reasons for strength degradation of structural ceramic materials is stress corrosion cracking. Caused mainly by water in the environment, stress corrosion cracking results in subcritical crack growth that leads to delayed failure of ceramic materials. As a consequence of this crack growth, ceramic components that are subjected to external stresses are liable to fail after an indeterminate period of time, leading to a considerable uncertainty in the safe design stress. One of the objectives of modern ceramics technology is to reduce the uncertainty associated with structural design, and hence, to improve our capabilities of designing ceramic components that exhibit reliable mechanical behavior. This objective can be accomplished in part through a better understanding of the fundamental processes that occur during stress corrosion cracking.

Subcritical crack growth occurs in almost every structural ceramic and is the prime cause of failure of these materials. From a phenomenological point of view we know that subcritical crack growth occurs in the presence of certain environments, usually water, and that the relationship between crack velocity and the stress intensity at the crack tip, as measured by a fracture mechanics test, takes the form shown in Figure 1.[1] We also have basic ideas about the mechanisms that control the fracture behavior of various ceramic materials. For instance, we know that in the part of the curve marked Region 1, growth is controlled by the rate of reaction of water with the material at the crack tip. In Region II, growth appears to be controlled by the rate of diffusion of water to the crack tip. There are a number of questions regarding the mechanisms of crack growth in other regions. For instance,

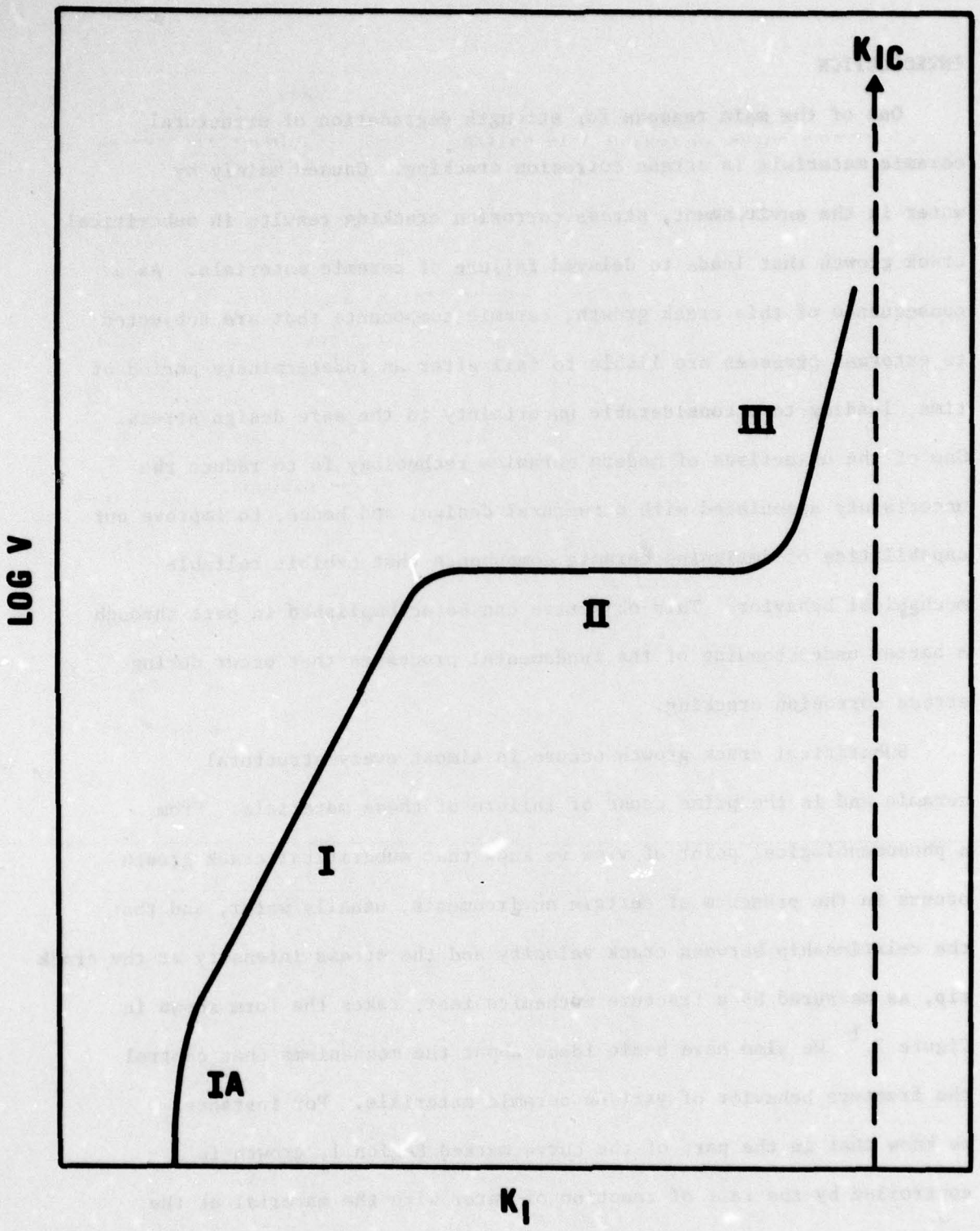

Figure 1. Schematic of a typical crack velocity - K_I curve for glasses and ceramics.

in Region III we know that crack growth is independent of the presence of water in the test environment. However, it has been shown that the crack growth curve in region 3 is shifted if the experiment is carried out in normal alcohols of various chain lengths[2]. The mechanism by which these alcohols effect the crack growth behavior is unknown at the present time. Another region of the curve, marked 1A, is observed only for certain glass compositions in particular environments[3]. This region has been attributed to a stress corrosion limit in these glasses. Why the relatively sharp break in the curve occurs, and how the mechanism of corrosion changes from regions 1A to 1 is not understood.

Most of the detailed studies of crack growth and stress corrosion cracking have been carried out in glasses because they are continuous, isotropic materials. A variety of models have been proposed to explain crack growth behavior in these materials. These models include diffusion controlled crack growth[4-6], and alkali ion mobility controlled generation of cracking within the glass[7]. Because it fits the experimental data over the widest range of conditions, the model most widely accepted to date is that of Hillig and Charles[8]. Their theory expresses the crack growth rate, v, in terms of an activated corrosion reaction at the crack tip:

$$v = v_o \exp\left(-E^* + V^*\sigma/3 - V_m\gamma/\rho\right)/RT \qquad (1)$$

Where E^* is the stress free activation energy, V^* the activation volume, σ the crack tip stress, V_m the molar volume, γ the interfacial surface energy between the glass and the reaction products, and ρ the radius of curvature of the crack tip. Based on this model, the temperature dependence of crack growth rates in glasses leads to activation energies which have been explained in terms of the reaction rate of silica with water[8]. While this chemical reaction seems

reasonable, questions arise as to the effect of the modifying ions in the glass compositions, i.e., alkali and alkaline earth ions, in the process. Specifically, is the exchange of a proton in the water for an alkali ion in the glass the first step in the stress corrosion process? The extent to which stress affects reaction rates is not known. However, tensile stresses have been shown to increase the hydrolysis of SiO_2.[9] Correspondingly, compressive stress was shown to decrease the hydrolysis rate. Experimental studies have shown that crack growth behavior does not vary in any simple way with glass composition[2]. Glasses that contain more alkali ions (which presumably weakens the silicon oxygen bonding), do not exhibit crack growth rates that are greater than glasses that contain lesser amounts of alkali.

Wiederhorn et. al.[10] showed that certain glasses exhibit slow crack growth even in vacuum ($\sim 10^{-5}$ torr), whereas others did not. These authors showed that fracture behavior of glasses in vacuum could be related to properties such as thermal expansion coefficient and compressibility. The relation between glass structure and crack growth behavior, however, is not understood.

A further impediment to our understanding of stress-corrosion cracking is the fact that subcritical crack growth is observed in such widely diverse materials as graphite, arsenic trisulfide and calcium fluoride. The mechanism of stress corrosion cracking in these materials is not understood, although we do know that crack growth rates are a function of stress intensity and that the data can be plotted in the same way as for glasses. In virtually every case noted above, moisture in the environment is the agent causing subcritical crack growth.

To fully understand the phenomenon of crack growth in ceramics, one must bring to bear new experimental techniques that can lead to an understanding of the corrosion behavior of ceramics. It is this corrosion behavior (i.e., the reaction of the environment with the material) that ultimately leads to stress corrosion cracking. Obviously, knowledge of the role of stress on the corrosion reaction is equally essential to enhance our understanding of stress corrosion cracking.

The following series of experiments was chosen to allow us to model the stress corrosion process at a crack tip as closely as possible. As far as we know, actual crack tips remain inacessible to existing characterization techniques, with the possible exception of Raman Spectroscopy which will be discussed later. Given this, it is our opinion that processes occurring on a fresh thin film approximate those at a crack tip. Spurious effects of environment can be eliminated by employing an experimental procedure whereby a thin film is formed, subjected to stress corrosion and analyzed without exposing it to an external environment. The use of a pristine film also allows one to load the surface to a high stress ($\sim 10^5$ psi), so as to enhance the stress corrosion process.

Electron spectroscopy for chemical analysis, ESCA, was chosen as the primary surface analysis tool because it samples the first 10Å of the surface, giving changes in bond energies. The energies of photoelectrons ejected from the surface due to the impingement of X-rays are analyzed. Shifts are observed in the energy of the emitted photons depending on the bond state of the atoms investigated. ESCA has been used quite extensively to study surface absorption of gases. ESCA can actually "look through" an absorbed layer to see both the surface and the absorbate. In addition, it has been found to be able

to distinguish between the silicon bridging-oxygen and the silicon non-bridging oxygen bonds in reacted glass.[11] Other surface analysis techniques including SIMS, ISS, and Auger spectroscopy can be used in conjunction with ESCA to give additional information.

Another potential source of information on stress corrosion in thin glass films is laser Raman spectroscopy. Studies of silica samples with varying water content have led to the identification of spectral features associated with the silicate hydroxyl group (=Si-OH)[12], and effect of chemical environment, stress, and temperature on these features would provide direct information on the hydrolysis of the silicon-oxygen bond.

Finally, crack growth studies themselves can yield results leading to the elucidation of stress corrosion mechanisms. Specifically, it will be shown in the following section that changes in the position of the Region II plateau can be used to determine the phenomenon controlling crack growth rates in this region.

Model for Diffusion Controlled Crack Growth in Brittle Materials

S. W. Freiman, S. M. Wiederhorn and C. J. Simmons

Work by Wiederhorn[1] showed that, in general, both glasses and ceramics exhibit multiple regions of subcritical crack growth in the presence of water as shown in Figure 1. Based on the work of Wiederhorn[1] who studied glasses in moist air as well as that of Freiman[2] who studied crack propagation in glasses immersed in alcohols, it is known that crack growth in Region I is governed by the rate of reaction of water in the environment with the material at the crack tip. Since the reaction is controlled by the chemical potential of water at the crack tip, the important parameter is the partial pressure of water i.e. relative humidity, in the environment. Region III crack growth is independent of water, but is affected by the alcohol chain length[2]. Region II has been postulated to be controlled by the rate of diffusion of water to the growing crack tip. As such, crack velocities should be relatively independent of stress intensity, as has been observed, and should be dependent on the rate of diffusion of water in the particular environment. A model for diffusion of water to a crack tip in a liquid or gaseous medium can be derived as follows.

Crack growth as controlled by the diffusion of water to the crack tip is shown schematically in Figure 2. Classically, a diffusion rate, can be expressed as

$$\mu = D \frac{dc}{dx} \tag{2}$$

where D is the diffusivity of water in the medium of interest and $\frac{dc}{dx}$ is the concentration gradient. If a linear gradient is assumed as shown in Figure 2, then Eq (2) can be shown to lead to

$$\mu = \frac{D\, C_{bulk} - C_{crack\ tip}}{\delta} \tag{3}$$

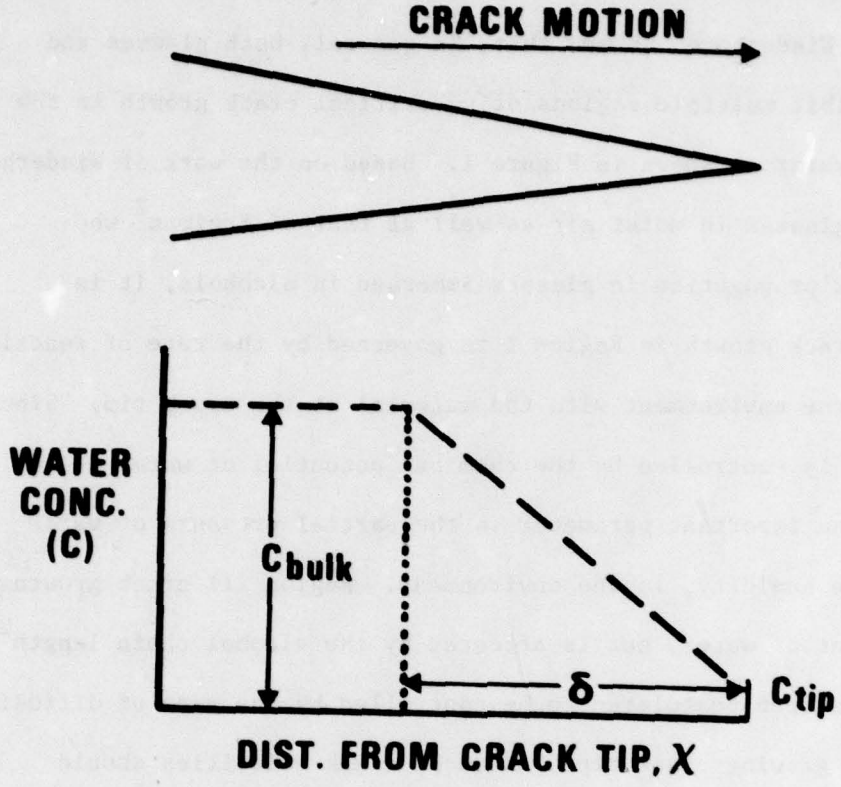

Figure 2. Assumed concentration gradient at a crack tip.

where δ is the width of the concentration gradient at the crack tip. Based on the Stokes-Einstein relation, D is given by:

$$D = \frac{kt}{6\pi r\zeta} \tag{4}$$

where k is the Boltzman constant, T the temperature, r the radius of the diffusing ion or molecule and, ζ the viscosity of the solution. Combining Eq's (3) and (4) and assumming that water is used up at the crack tip, so $C_{bulk} >> C_{crack\ tip}$ yields:

$$\mu = \frac{kt}{6\pi r} \frac{C_{bulk}}{\zeta} \tag{5}$$

Assuming that crack velocity is proportional to diffusion rate in region 2

$$v \alpha \mu = \frac{Akt}{6\pi r} \frac{C_{bulk}}{\zeta} \tag{6}$$

where A is an empirical constant.

Experimental Procedure

The experimental study was undertaken to determine the applicability of the above model to water diffusion controlled crack growth in straight chain alcohols. A series of alcohols ranging from butanol to decanol were allowed to sit over water for a long period of time (years) in order to saturate the alcohol. Crack growth studies were conducted in each of these alcohols employing the load relaxation technique on soda lime silica glass, double torsion, specimens. Crack velocities were obtained over the range 10^{-6} to 10^{-3}m/sec. Crack velocities below 10^{-6}m/sec could not be obtained by this technique because of thermal fluctuations in the Instron test machine. Water concentrations in the alcohols were determined by the Karl-Fischer technique. The viscosities of the alcohol-water solutions were obtained approximately the same temperature at which the crack growth data was taken, using a Cannon-Fenske kinematic viscometer.

Results and Discussion

The crack growth data in the various alcohols is presented in Figure 3. Except for a reversal of octyl and decyl alcohols, due to the fact that the octyl alcohol was not saturated with water, there is a general increase in the velocity of the Region II plateau with decreasing alcohol chain length. The positions of both Region 1 and Region III appear to agree with previous data[2] although some shift due to differences in test technique are to be expected.

The region 2 behavior is shown in more detail in Figure 4, in which the plateau crack velocities at a K_I of 0.62 for each of the alcohols, is given as a function of alcohol chain length. According to Equation 6, the Region II crack velocity should be directly proportional to water concentration and inversely proportional to viscosity. That such a model fits this crack growth data is shown in Figure 5. Considering the fact that crack velocity is plotted on a linear scale, the fit of the data to the model is quite good. That it is the concentration of water in an alcohol, and not the partial pressure, that controls crack velocities in Region II is shown by the fact that two alcohols such as butyl and amyl, both of which are water saturated but whose solubility for water is different, have different Region II plateaus. The increase in the Region II crack velocity plateau with increasing water content in three different alcohols is shown in Figures 6 through 8. It is seen that in ethyl alcohol, which is mutually soluble with water over the entire composition range, the Region II can be displaced to such high levels that it is not observed.

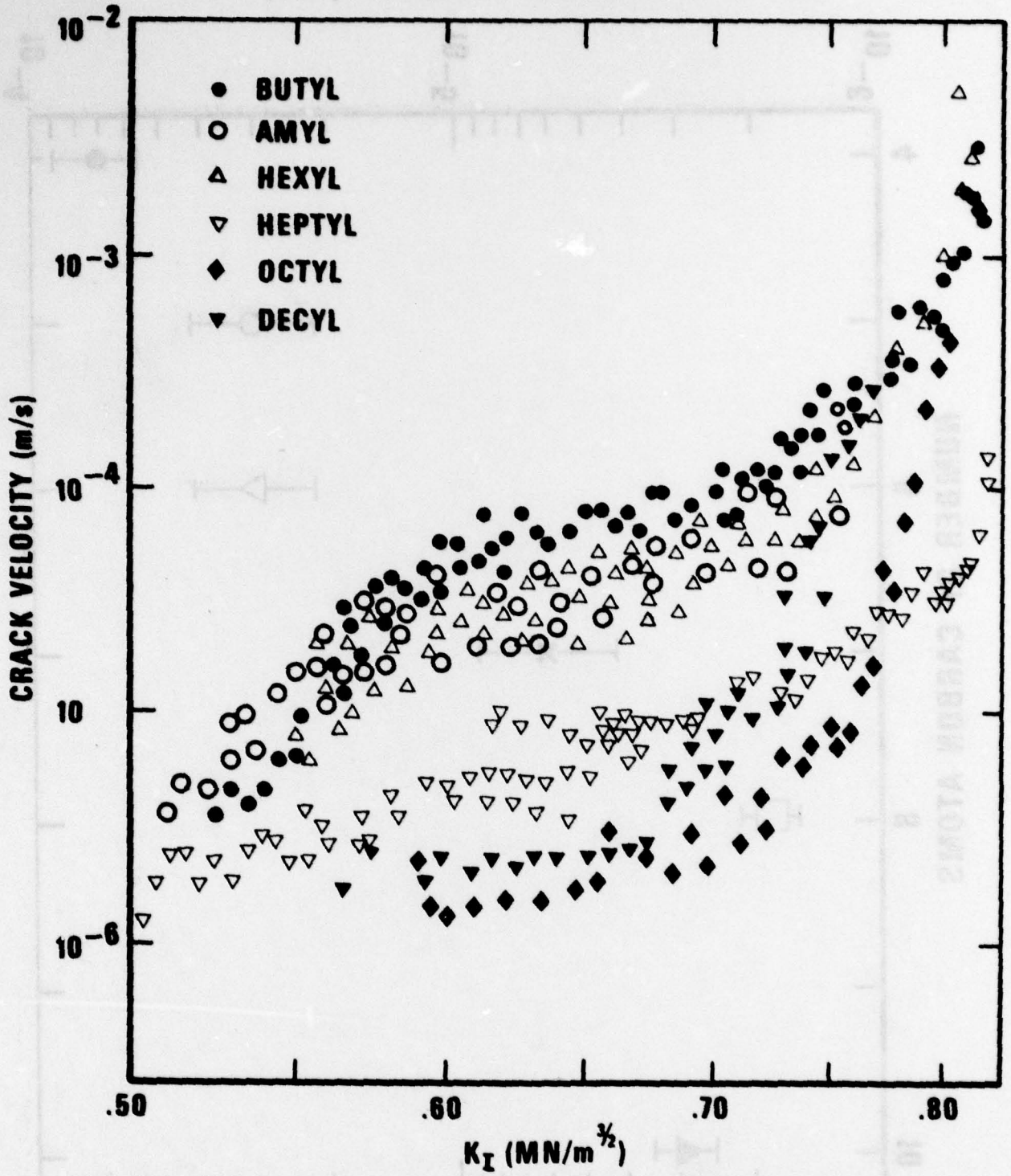

Figure 3. Crack velocity data for soda-lime glass tested in various straight chain alcohols; points represent only a portion of the data acquired.

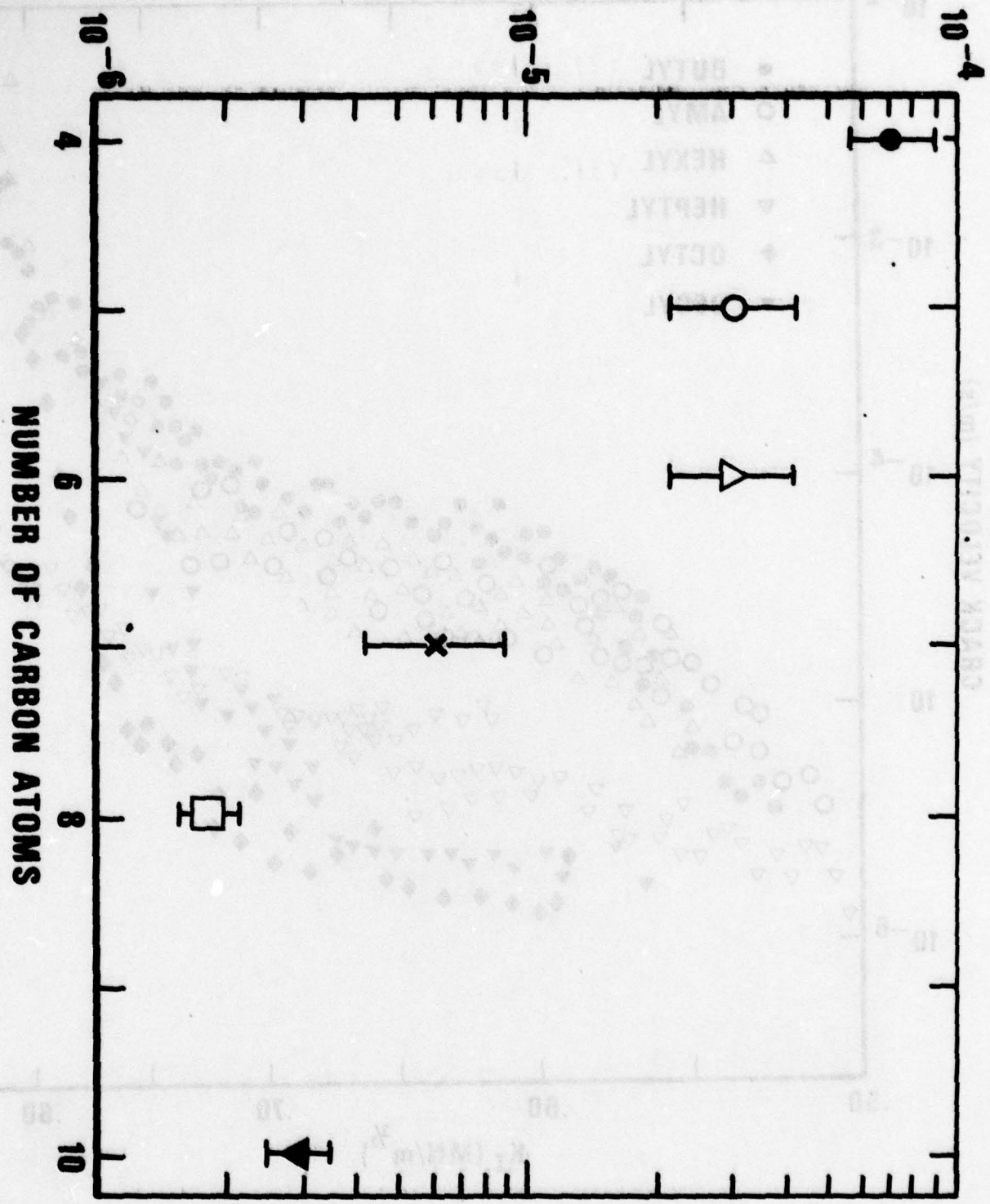

Figure 4. Crack velocity as a function of alcohol chain length taken at a K_I of 0.62 MPa $m^{\frac{1}{2}}$.

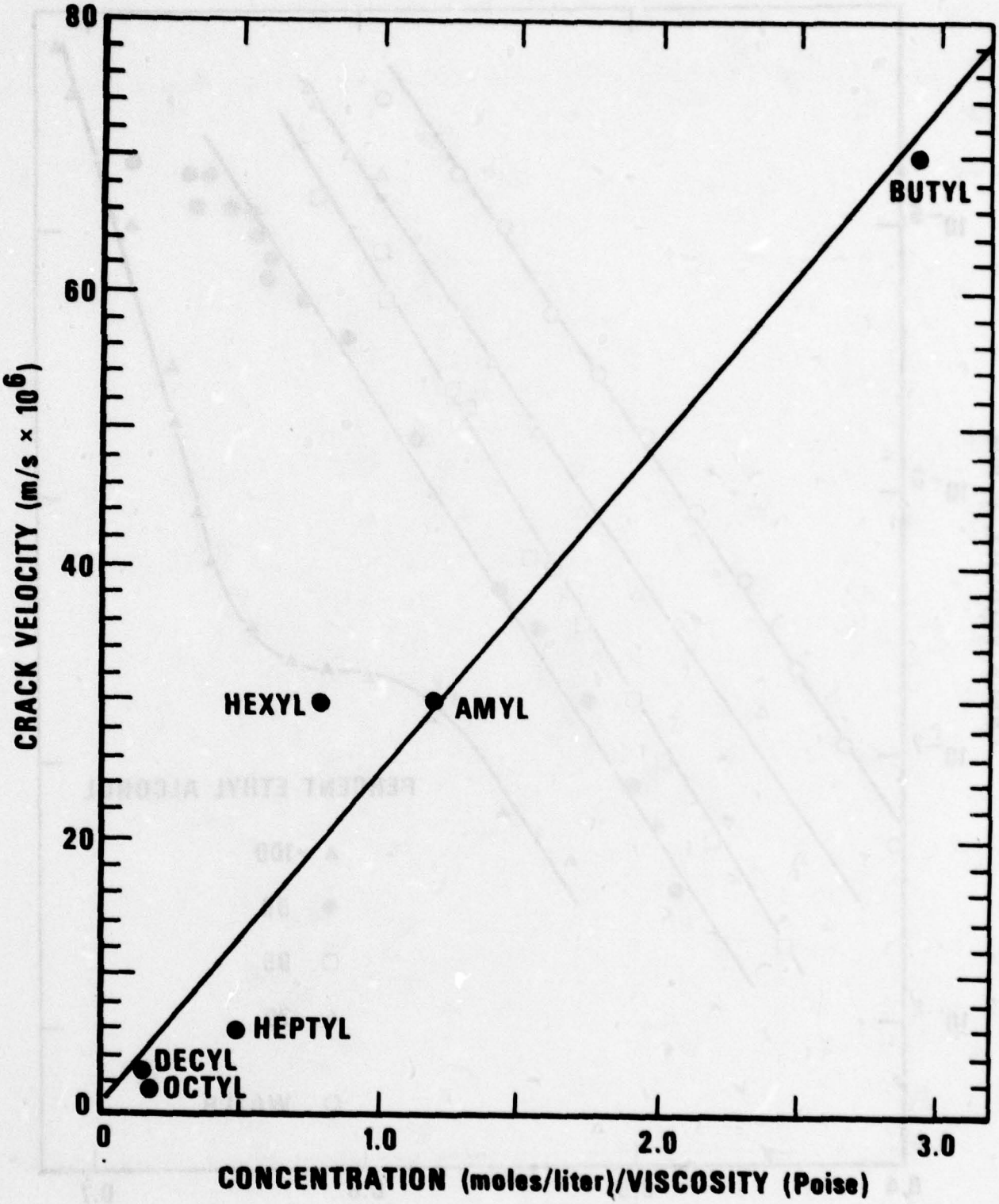

Figure 5. Crack velocity plotted as a function of water concentration/viscosity according to Eq. 6.

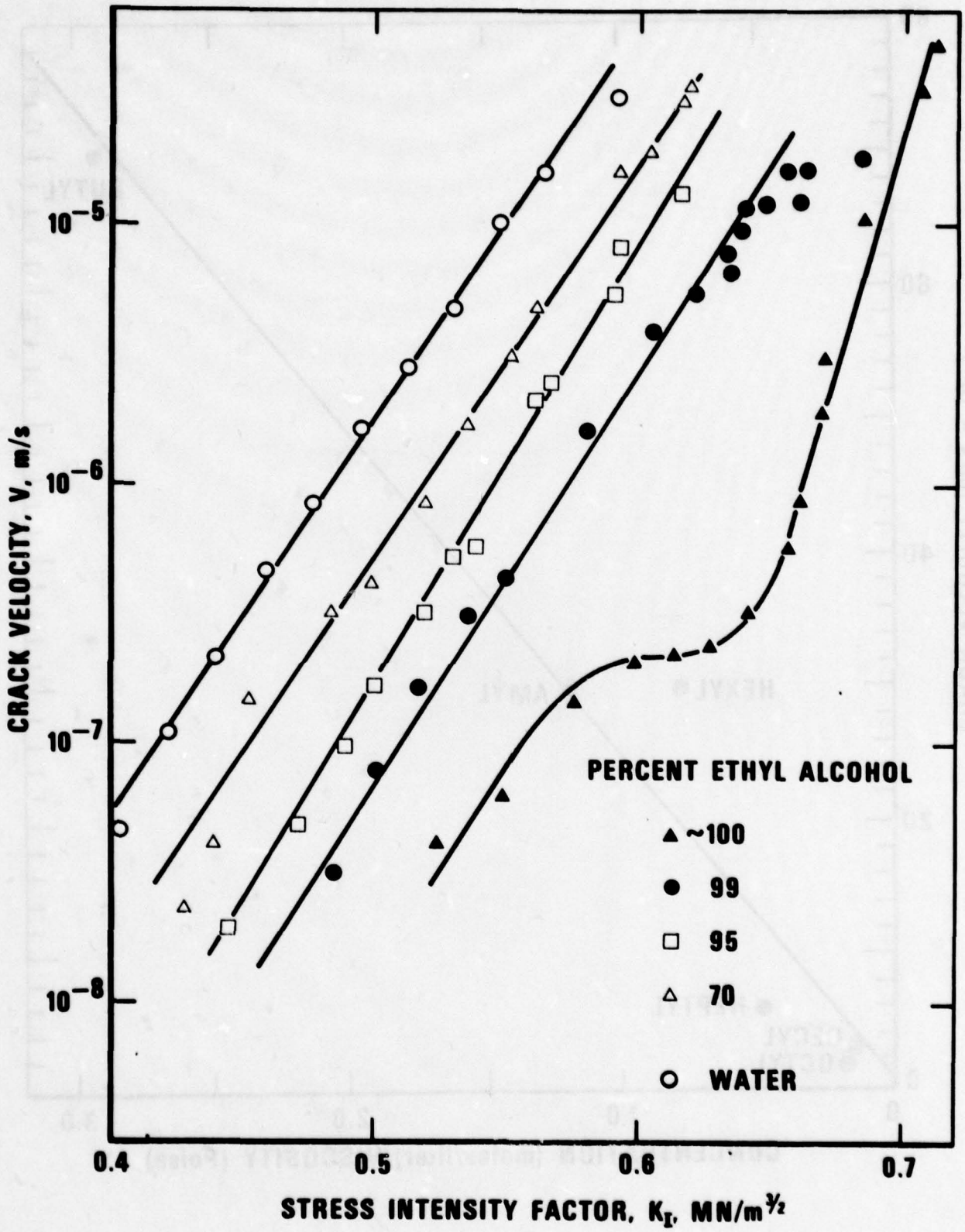

Figure 6. Crack velocity data in soda-lime glass measured in ethyl alcohol containing various quantities of water.

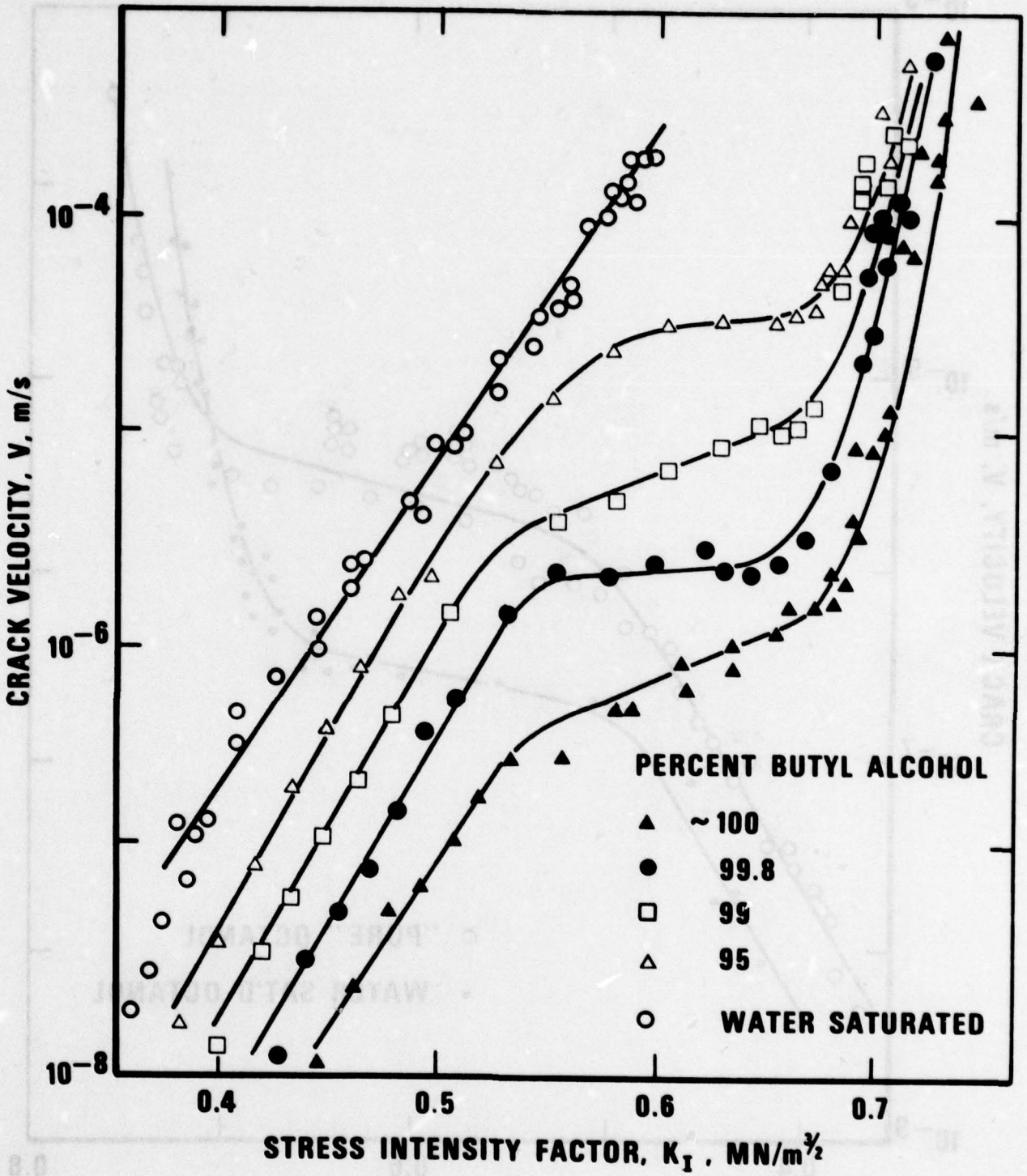

Figure 7. Crack velocity data in soda lime glass measured in butyl alcohol containing various quantities of water.

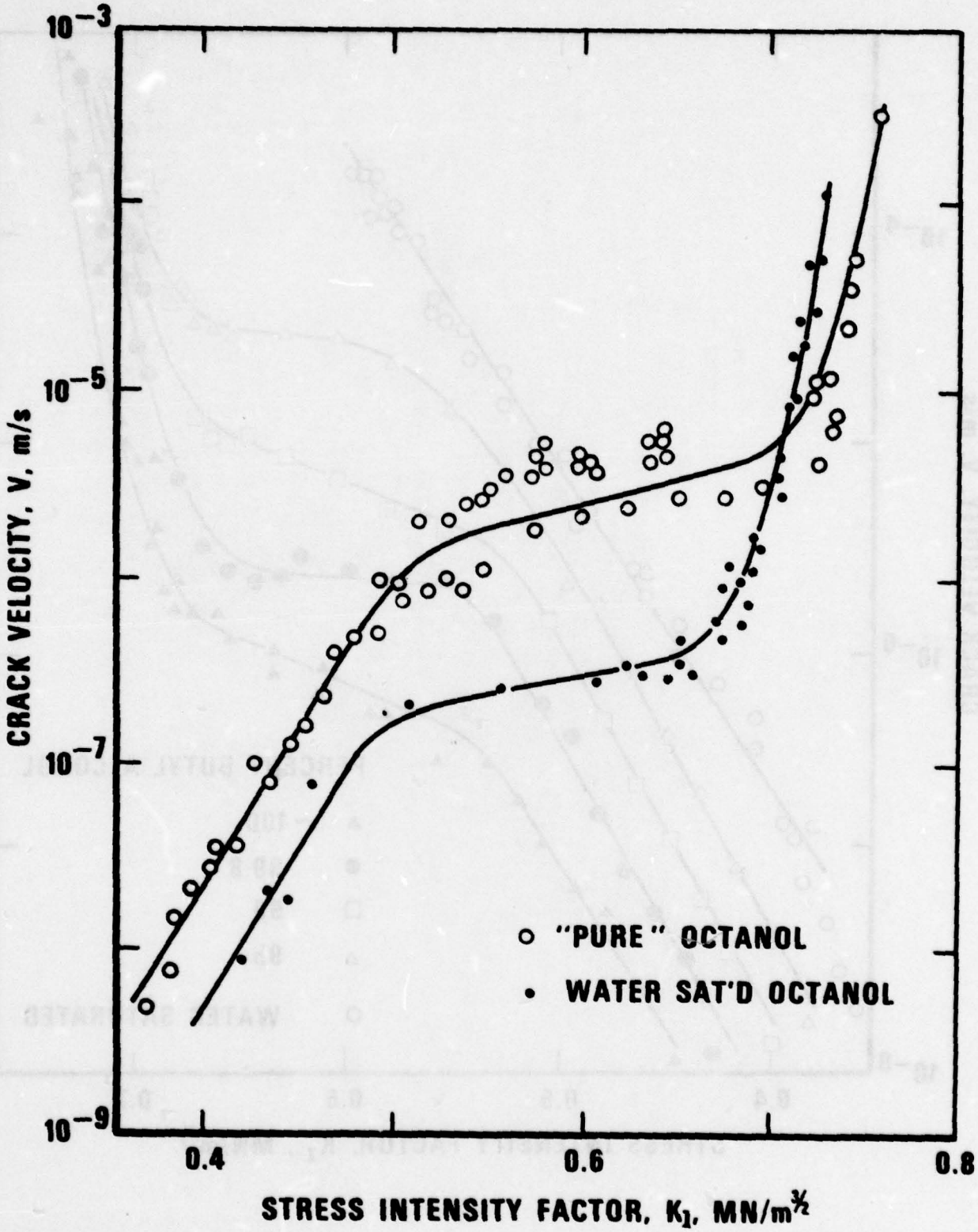

Figure 8. Crack velocity data in soda lime glass measured in either "pure" octyl alcohol or octyl alcohol saturated with water.

EFFECT OF REGION II CRACK PROPAGATION ON PROOF TESTING

S. M. Wiederhorn, E. R. Fuller, Jr. and S. W. Freiman

An experimental and theoretical investigation has been initiated to study the effect of region 2 crack growth behavior on proof-testing. This study was initiated because an earlier theoretical investigation of proof-testing in a stress-corrosion medium suggested a significant dependence of the strength distribution after proof-testing on the stress corrosion medium. If the strength distribution before proof can be represented by a two parameter Weibull equation:

$$\ln (\ln (1-f)^{-1} = m \ln (S/So), \qquad (7)$$

where F is the cumulative failure probability and S is the strength, and if the crack growth rate, v, can be expressed as a power function of the applied stress intensity factor, K_I:

$$v = A K_I^n, \qquad (8)$$

then the strength can be represented by two Weibull curves, one with a slope of m at high cumulative failure probability levels, the other with a slope of m-z at low failure probability levels. m and So are usually determined from a least squares fit of strength data. Truncation of the strength distribution always occurs as a result of proof testing; the truncation strength depends on the rate of unloading.

In contrast to the above prediction for single region crack propagation, multi-region crack propagation (Figure 1) results in a more complicated strength distribution after proof testing. Depending on the loading rate and the test environment, bimodal strength distributions occur as a result of proof testing. This effect was shown to be a consequence of Region II crack propagation (the plateau in Figure 1), which severely distorts the

strength distribution curve resulting from proof testing. With regard to assuring component reliability, a distrubing aspect of Region II crack propagation is that for equivalent failure probabilities, portions of the strength distribution after proof testing lie at lower load levels than the initial distribution (Figure 9), resulting in significant probabilities of failure at low loads after proof testing. This effect is predicted from the theory for both dry and moist environments, however, experimental comfirmation of the effect has not yet been obtained. Consequently, an experimental objective of the present study is to demonstrate this effect of region II crack growth on proof testing.

To test the effect of Region II crack propagation, proof-tests are being conducted in heptane on soda-lime-silicate glass slides. Heptane has been selected as a test medium because crack growth studies indicate a wide range of values of the stress intensity factor for region II crack growth in this fluid.[13] Thus, the effect, should be exaggerated in heptane. A computer program, which gives theoretical predictions of the effect, is being used to establish experimental conditions for the laboratory tests. Based on experimental crack growth studies obtained by Freiman,[13] cracks propagating in heptane pass through a wide region of diffusion controlled crack growth. Soda lime glass tested in heptane should provide unequivocal regarding effects of region II crack growth on post proof test strength distributions.

Based on test conditions predicted from the computer simulation, proof tests in heptane were conducted on 134 microscope slides. Of these 21 (15.7 percent) broke during the proof test cycle, where as the predicted failure rate based on 283 strength measurements was ∿40 percent. While this difference cannot be explained with certainty at this time, it may result from uncertainties either in the Weibull parameters for

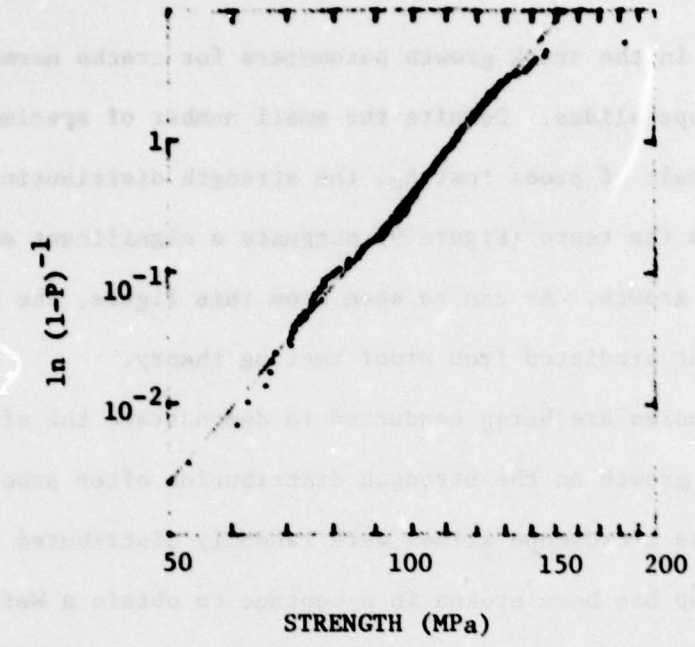

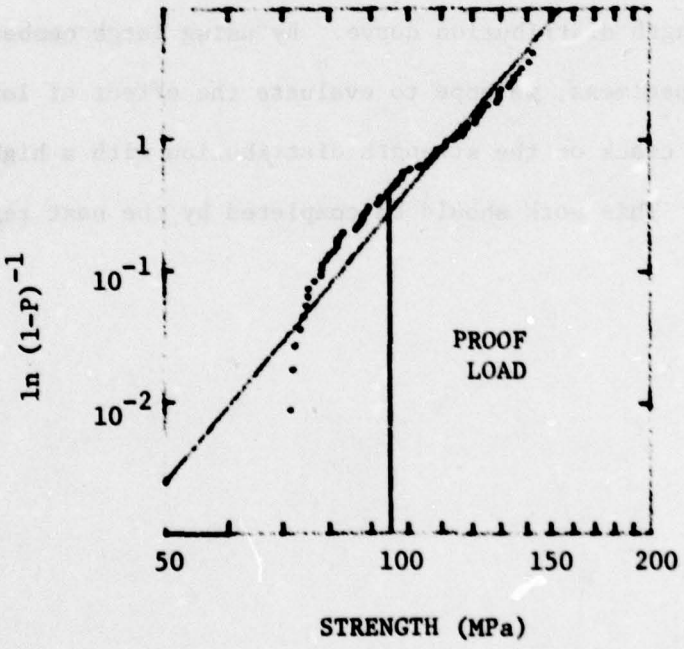

Figure 9. Strength distributions of soda-lime glass microscope slides before (a) and after (b) proof testing. Both strength tests and proofing were performed in heptane.

the lot tested, or in the crack growth parameters for cracks normally present in microscope slides. Despite the small number of specimens that broke as a result of proof testing, the strength distribution curve obtained from the tests (Figure 9) suggests a significant effect of Region II crack growth. As can be seen from this figure, the shape of the curve is that predicted from proof testing theory.

Additional studies are being conducted to demonstrate the effect of Region II crack growth on the strength distribution after proof testing. 2500 glass microscope slides were randomly distributed into 8 groups. One group has been broken in n-heptane to obtain a Weibull distribution for the 2500 slides. The other groups will be subjected to specific proof test cycles and then broken to evaluate the effect of proof testing on the strength distribution curve. By using large numbers of randomly selected specimens, we hope to evaluate the effect of load cycle and region II crack on the strength distribution with a high degree of accuracy. This work should be completed by the next report period.

EFFECT OF STRESS ON THE RAMAN SPECTRA OF GLASS

P. N. Krishnan, S. W. Freiman and G. E. Walrafen

The vibrational spectra of the atoms in a solid provide information regarding their bonding and chemical environment in the material. Raman spectroscopy is one technique for obtaining this information. The Raman spectra of fused silica (Figure 10) contains lines at $490cm^{-1}$ and $604cm^{-1}$ which have been attributed to defects of the form:

---Si---O...Si

where O···Si represents a broken Si-O bond.[11] It has been hypothesized that water can be preferentially trapped at these defect sites resulting in the structure:

---Si - OH HO - Si

The presence of water at the defect changes the intensity of the $490cm^{-1}$ and $604cm^{-1}$ lines relative to the other lines in the spectrum. If water reacts with silica at a crack tip under stress, then the intensity of these lines should be magnified at the crack tip compared to the same lines in a spectrum taken from the bulk glass.

The ratio of the intensities of the lines at $490cm^{-1}$ and $440cm^{-1}$ (I_{490}/I_{440}) was obtained using a laser with an exciting line of $5145cm^{-1}$, at both a crack tip wedged open using the set-up shown in Figure 11, as well as in the bulk fused silica. If there were no effect of the crack tip then the ratio of (I_{490}/I_{440}) crack tip to (I_{490}/I_{440}) bulk should be 1. All reliable results to date have indicated that the above ratio is 1.005 to 1.01 but never ≤ 1. While indicating promise, these results are inconclusive. One problem is that the laser beam area is quite large compared to the region of high stress at the crack tip. Estimates of the

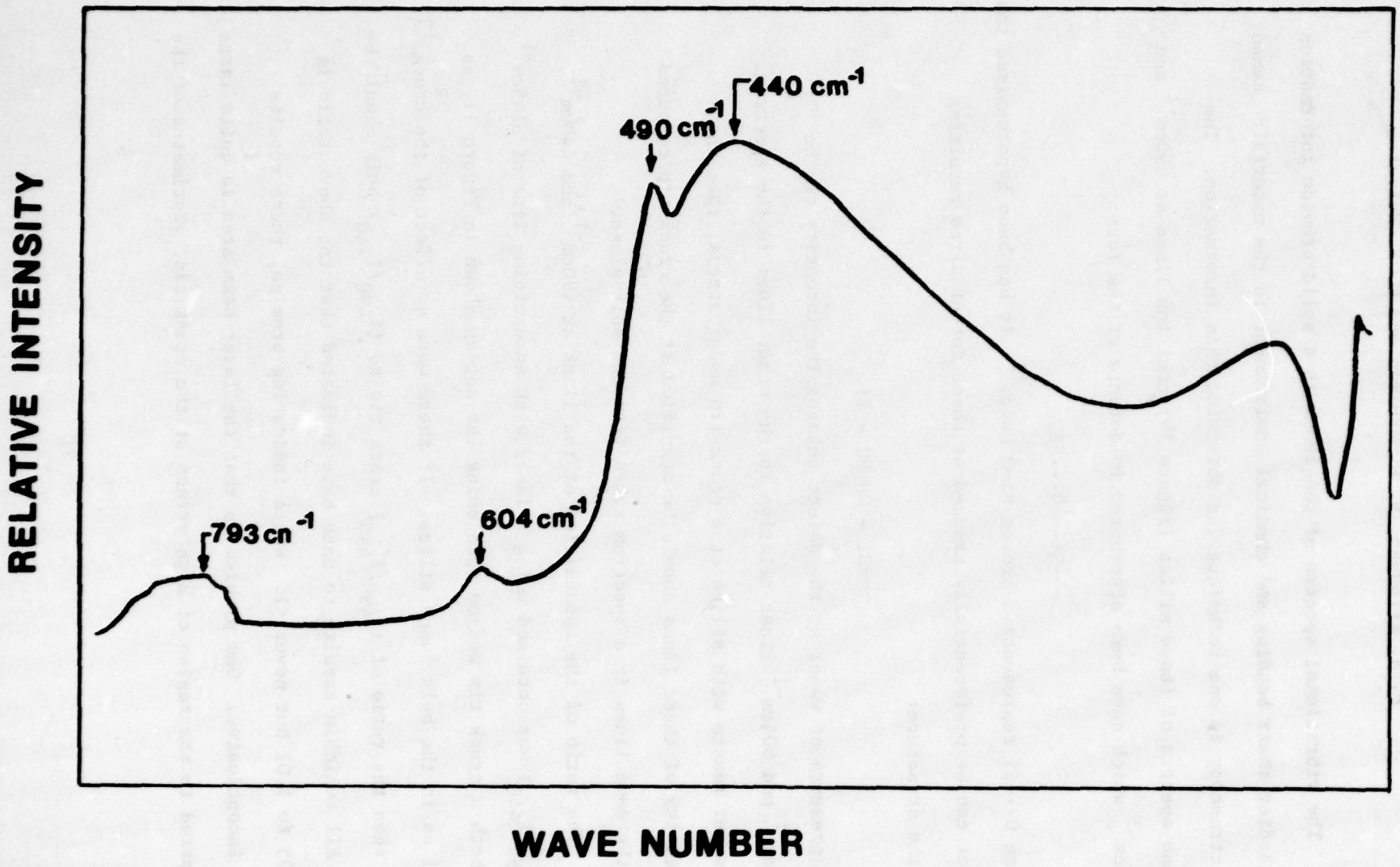

Figure 10. Raman spectrum of fused silica (G.E. 151). Peaks at 490 cm^{-1} and 604 cm^{-1} have been associated with defects in the SiO_2 structure.

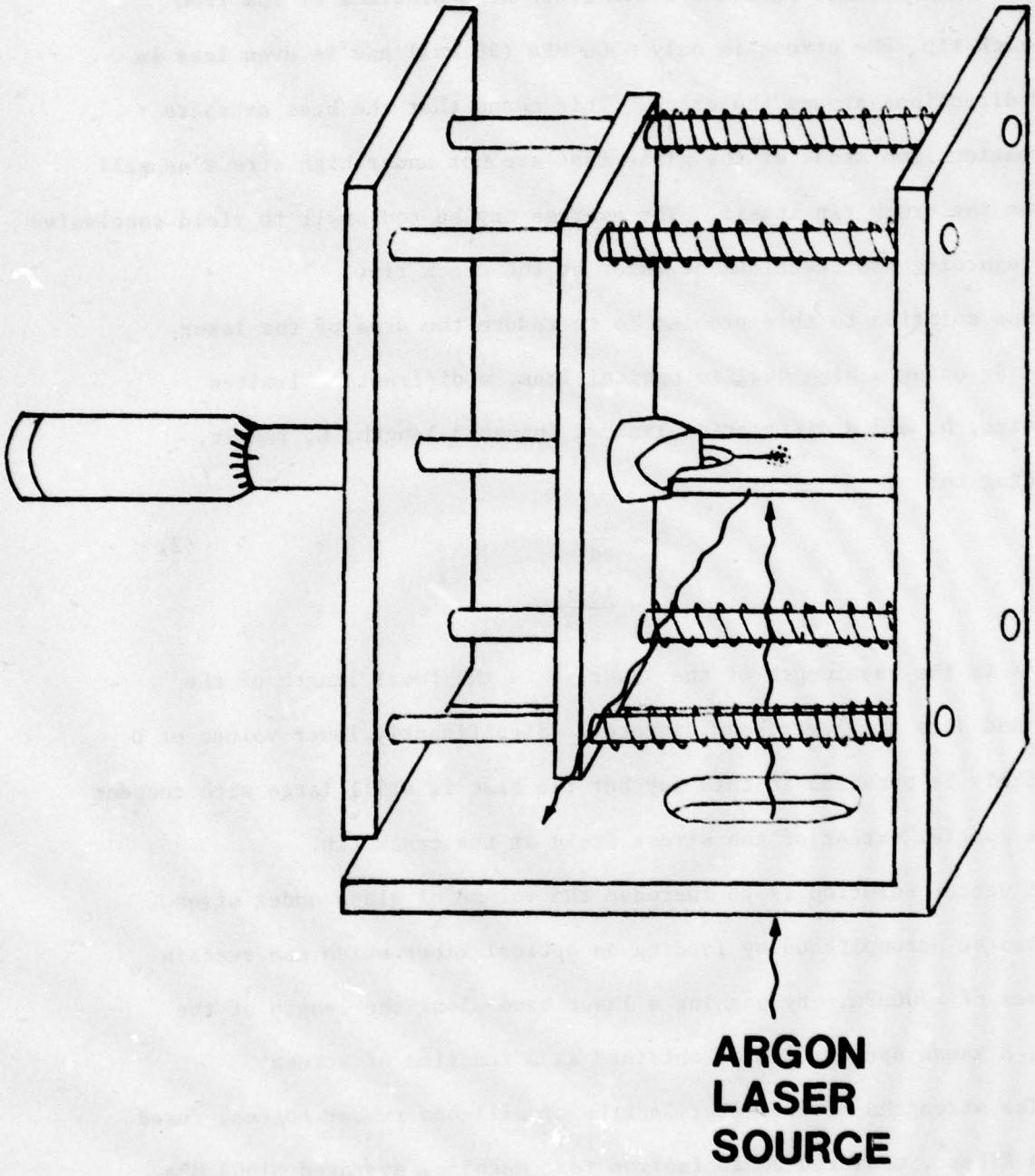

Figure 11. Wedge loaded specimen for use in Raman Spectroscopy System. Laser beam is focused in $\sim$1 mm^2 area at the crack tip or in the bulk.

stress, σ_{CT} in the crack tip plane were made from:

$$\sigma_{CT} = \frac{K_I}{\sqrt{2\pi r}} \qquad (1)$$

where K_I is the stress intensity at the crack tip (estimated to be 0.7) and r is the distance from the crack tip. At a distance of 1μm from the crack tip, the stress is only ∿300 MPa (50 ksi) and is even less in other directions around the crack. This means that the beam extracts information from areas of the glass that are not under high stress as well as from the crack tip itself. The average may be too small to yield conclusive data regarding the reactions of water at the crack tip.

One solution to this problem is to reduce the area of the laser beam. By using a high quality optical lens, a diffraction limited spot size, D, and a diffraction limited focussed length, L, result, according to:

$$D = \frac{4\lambda f}{\pi d} \qquad (2)$$

$$L = \frac{16\lambda f^2}{\pi d^2}$$

where λ is the wavelength of the laser, f is the focal length of the lens, and d is the laser beam diameter. Significantly lower values of D can likely be obtained in this way but the size is still large with respect to the spatial extent of the stress field at the crack tip.

A better solution is to increase the volume of glass under stress. This can be accomplished by loading an optical fiber which can sustain stresses of >700MPa. By passing a laser beam along the length of the fiber, a Raman spectra can be obtained as a function of stress.

The strengths of 0.5 meter lengths of silicone rubber coated, fused silica fiber*, measured on an Instron test machine, averaged ∿1500 MPa. About 30 meters of this fiber was suspended from a stairwell. A weight was hung from the fiber to yield a stress of ∿700 MPa. The stressed

---

*Optelcom, Inc.

fiber was carefully wound onto a specially constructed aluminum drum. The drum was turned by hand at a constant speed in order to keep a uniform stress on the fiber. Two rubber coated clips were attached to the drum to keep the fiber in place. Raman spectra of the fiber were obtained using a slitless optical fiber laser-Raman spectrometer at Tracor Corp., Rockville, MD. Argon ion laser excitation at 5145A° was employed at a power of 500 MW. The exciting radiation was blocked at the exit end of the fiber by a Corning 3-69 filter. A scrambler was not used because the fiber itself scrambles the polarization.

Qualitatively, it was observed that the intensities of the bonds at $490cm^{1}$ and $604cm^{1}$ were greater in the stressed fiber than in the same fiber after the stress was removed. The quantitative determination of (I_{490}/I_{440}) is awaiting the determination of a more accurate baseline for the stressed and unstressed spectra. Longer fibers under higher stresses are now being used in order to enhance the phenomenon.

SURFACE ANALYSIS SYSTEM

D. M. Sanders and S. W. Freiman

As expected, work during this past year was largely devoted to the design and construction of an experimental facility which will permit the preparation and analysis of thin films of selected compositions, using simultaneous evaporation from three electron beam evaporation sources and up to seven heated boat sources. This apparatus, will consist of a surface analysis subsystem purchased from Leybold Heraeus Inc. coupled to an NBS designed deposition chamber by a carousel load lock chamber; the latter two designed and constructed at NBS. The final configuration of the facility is pictured in Figure 12.

Electron Spectroscopy for Chemical Analysis (ESCA) is the primary technique to be used to determine the nature of the chemical reactions responsible for delayed fracture phenomena. ESCA was chosen because of its ability, under favorable circumstances, to detect differences in the nature of the chemical bonding of the atoms near the surface. These differences are seen as shifts in the characteristic binding energies of the electrons surrounding the atoms in question. As outlined in Table 1, ESCA involves the measurement of the energy distribution of photoelectrons which are produced when the surface in question is irradiated with X-rays or ultraviolet light. The fundamental process leading to the production of these photoelectrons is well understood and hence quantitative analysis of all atoms except hydrogen is possible with a resolution in depth from the surface of 10-30 Å.

Due to favorable circumstances, the National Bureau of Standards was able to acquire a Surface Analysis System having other analytical

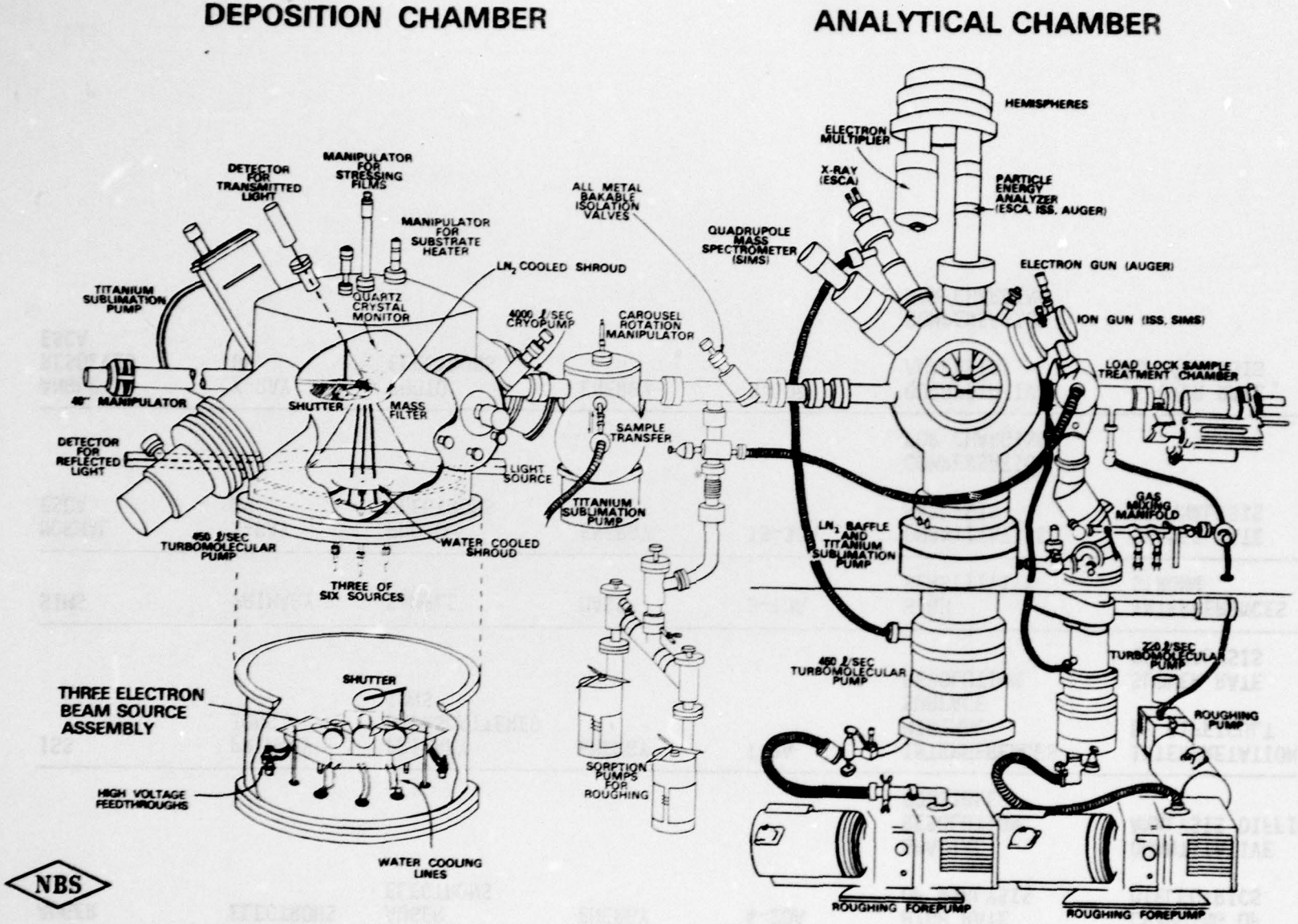

Figure 12. NBS deposition and surface analysis facility.

TABLE I. SURFACE ANALYSIS TECHNIQUES

TECHNIQUE	IN	OUT	ANALYZED BY	DEPTH OF ANALYSIS	ADVANTAGES	DISADVANTAGES
AUGER	ELECTRONS	AUGER ELECTRONS	ENERGY	4-20A	HIGH RATE OF ANALYSIS SPACIAL RESOLUTION POSSIBLE	CHARGING OF DIELECTRICS QUANTITATIVE ANALYSIS DIFFICULT
ISS	PRIMARY IONS	PRIMARY BACKSCATTERED IONS	ENERGY	1-3A	INTERFERENCES MINIMAL SURFACE RESOLUTION	INTERPRETATION CAN BE DIFFICULT SLOWER RATE OF ANALYSIS
SIMS	PRIMARY	SAMPLE	MASS	3-10A	HIGH SENSITIVITY	INTERFERENCES STRONG
NORMAL ESCA	X-RAY UV	PHOTO ELECTRONS	ENERGY	15-30A	QUANTITATIVE ANALYSIS COMPENSATION FOR CHARGING	SLOWER RATE OF ANALYSIS
ANGLE RESOLVED ESCA	X-RAY UV	PHOTO ELECTRONS	ENERGY	5-10A	QUANTITATIVE ANALYSIS COMPENSATION FOR CHARGING	SLOWER RATE OF ANALYSIS

techniques in addition to ESCA. This surface analysis subsystem was recently delivered and is pictured as part of the overall facility in Fig. 12. The surface analysis system consists of two interconnected but separately pumped vacuum chambers. The preparation chamber on the far right is part of a rapid entry loadlock for introduction of samples for analysis. It allows both deposition of thin films by single source thermal evaporation and by sputtering. There is also a gas manifold to allow introduction of reactive atmospheres. The preparation chamber is pumped using a 220 liter/sec turbomolecular pump and achieves an ultimate base vacuum of 1×10^{-9} m bar after baking to 250°C.

To the left of the preparation chamber is the main analytical chamber. This chamber is pumped using a 450 liter/sec turbomolecular pump, a liquid nitrogen baffle, and titanium sublimation pump reaching an ultimate base vacuum of 5×10^{-11} m bar. Provision is made in this chamber for all of the experimental techniques listed in Table 1, in addition to the ability to carry out rastered sputtering for depth profiling. These available techniques include ESCA, angle resolved ESCA, Secondary Ion Mass Spectroscopy (SIMS), Ion Scattering Spectroscopy (ISS), and Auger Electron Spectroscopy (AES). The three added techniques should prove extremely useful in the interpretation of the ESCA spectra because they provide complimentary information about the same area of the sample surface. The ISS technique, for instance, permits quantitative analysis of the first atomic layer of the sample surface. This layer would be the most susceptible to changes in composition during stress enhanced reactions. The ISS technique involves

measuring the energy of inelastically backscattered primary sputtering ions using the same hemispherical electrostatic energy analyser as is used for electrons when carrying out AES and ESCA, but electrically biased in the opposite sense.

The SIMS technique, on the other hand, involves the measurement of the ions which are sputtered from the sample surface by an ion beam using a specially designed prefilter--quadrupole mass spectrometer arrangement. This technique has extreme sensitivity for some ions and is unique in its ability to analyze surface hydrogen ions.

The preparation chamber, the entry port and the analytical chamber are all interconnected with a sample holding rod coupled with a differentially pumped metal sliding seals arrangement. A substrate can be introduced at the entry port on the far right (See Fig. 12) and transferred to either the preparation chamber of the Analytical Chamber without disturbing the vacuum in either. As will be discussed shortly, a substrate holding and stressing jig has been designed which fits in a cavity in the sample rod so that thin films can be deposited on the substrate by thermal evaporation or sputtering. The resulting thin film cam then be transferred to the analytical chamber for characterization without exposure to contaminating adsorbed gases. Once this pristine surface is analyzed, it can be returned to the preparation chamber where stress can be applied to the film by bending the substrate. The film can then be transferred to the analytical chamber where it is re-analyzed to determine if there are observable changes induced by stretching the chemical bonds at the surface. This characterization of the stressed state will serve as a basis for

comparison for future exposures of the newly prepared surface to reactive environments as a function of stress. These reactive environments will be introduced into the preparation chamber using the gas manifold arrangement. The resulting reacted film can then be re-introduced into the analytical chamber for further analysis to determine changes in the thin film surface caused by stress induced reactions.

A specimen holder which can be used to apply stress to a substrate on which a thin film has been deposited, has been built. As shown in Figure 13, this device is held in the traveling specimen rod. Stress is applied to the cantilevered substrate with a hexagonal screw which is turned using a linear-rotary manipulator. The width of the substrate is tapered to permit the application of a constant bending stress over the region of the specimen to be analyzed. By using a material which has a sufficiently high yield strength e.g. a 2% Be-Cu alloy, stresses of 700 MPa or greater can be applied to the substrate, putting stresses of the same or greater magnitude into the thin film (depending on the Young's modulus of each material). The stress can be applied during exposure to the controlled environment and can be removed or left on during surface analysis.

At this time techniques have been developed to permit the deposition of low melting point congruently vaporizing compositions such as magnesium fluoride in the Leybold Heraeus preparation chamber. It is possible to pre-melt chunks of this material in a separate vacuum chamber into a tungsten filament. When this filament is introduced into the preparation chamber and resistively heated, a thin film can be produced. This film can then be transferred to the analytical chamber without leaving ultra high vacuum conditions.

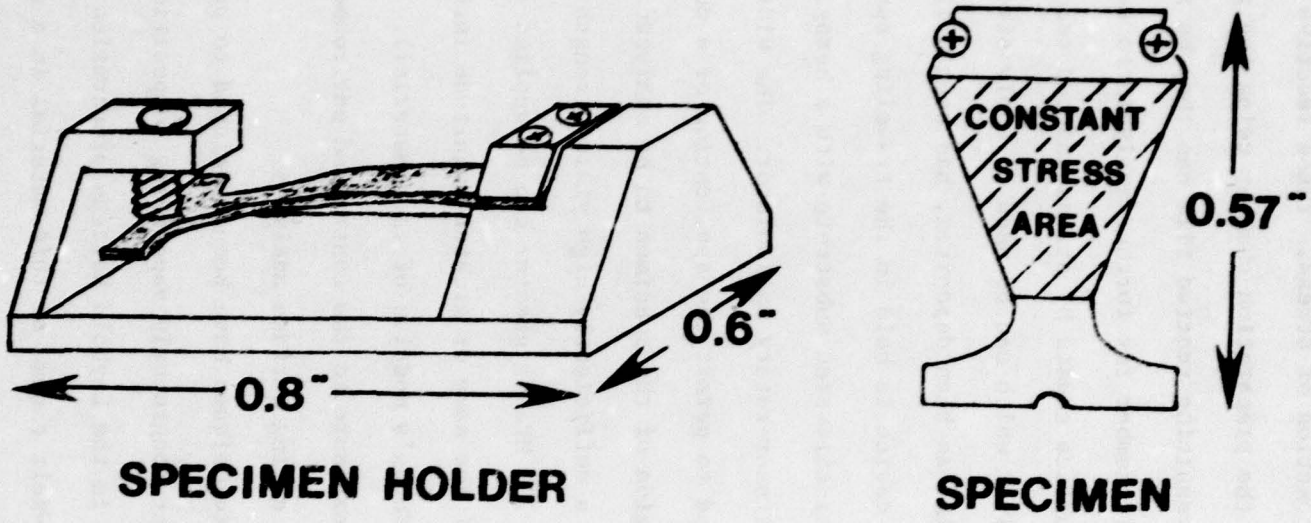

Figure 13. Substrate holder and substrate for thin film, stress corrosion experiments. Film is stressed by applying a force to the end of the cantilever substrate using a linear, rotary micromanipulator. Shaded area on substrate is at the same stress level.

Figure 14 shows an ESCA spectrum of a pristine magnesium fluoride film which was so produced and subsequently transferred into the analysis chamber. As expected, the major features in the spectrum are magnesium and fluorine photoelectron and Auge peaks. The existance of smaller peaks due to the stainless steel substrate holder remains to be varified.

While the approach outlined above has yielded preliminary experience with the preparation, stressing and analysis of thin films, it suffers from a severe restriction in the number of compositions of thin films which can be deposited. Since a primary objective of the study is delayed fracture reactions in a variety of ceramic materials of engineering interest, additional design and construction is being carried out to produce a deposition chamber having the unique combination of ultra high vacuum (10^{-10}m bar) coupled with provision for simultaneous co-evaporation from electron beam and thermal boat sources under mass spectrometer control. These sources include a three source electron beam module purchased from and recently delivered by Airco Temescal.

The deposition chamber consists of a stainless steel vacuum chamber with copper seal flanges to permit an ultimate vacuum after baking to 250°C of 1×10^{-10} m bar. The chamber is ultimately to be pumped using a liquid nitrogen shroud, two 1600 liter/sec He cycle Cryo-pumps, a 270 liter/sec turbomolecular pump and a 10,000 liter/sec titanium sublimation pump.

The internal fixturing of the deposition chamber has also been designed and constructed. These include the water cooled shroud directly over the thermal boat sources, the liquid nitrogen shroud directly under the substrate, the mirror inserts for optical monitoring

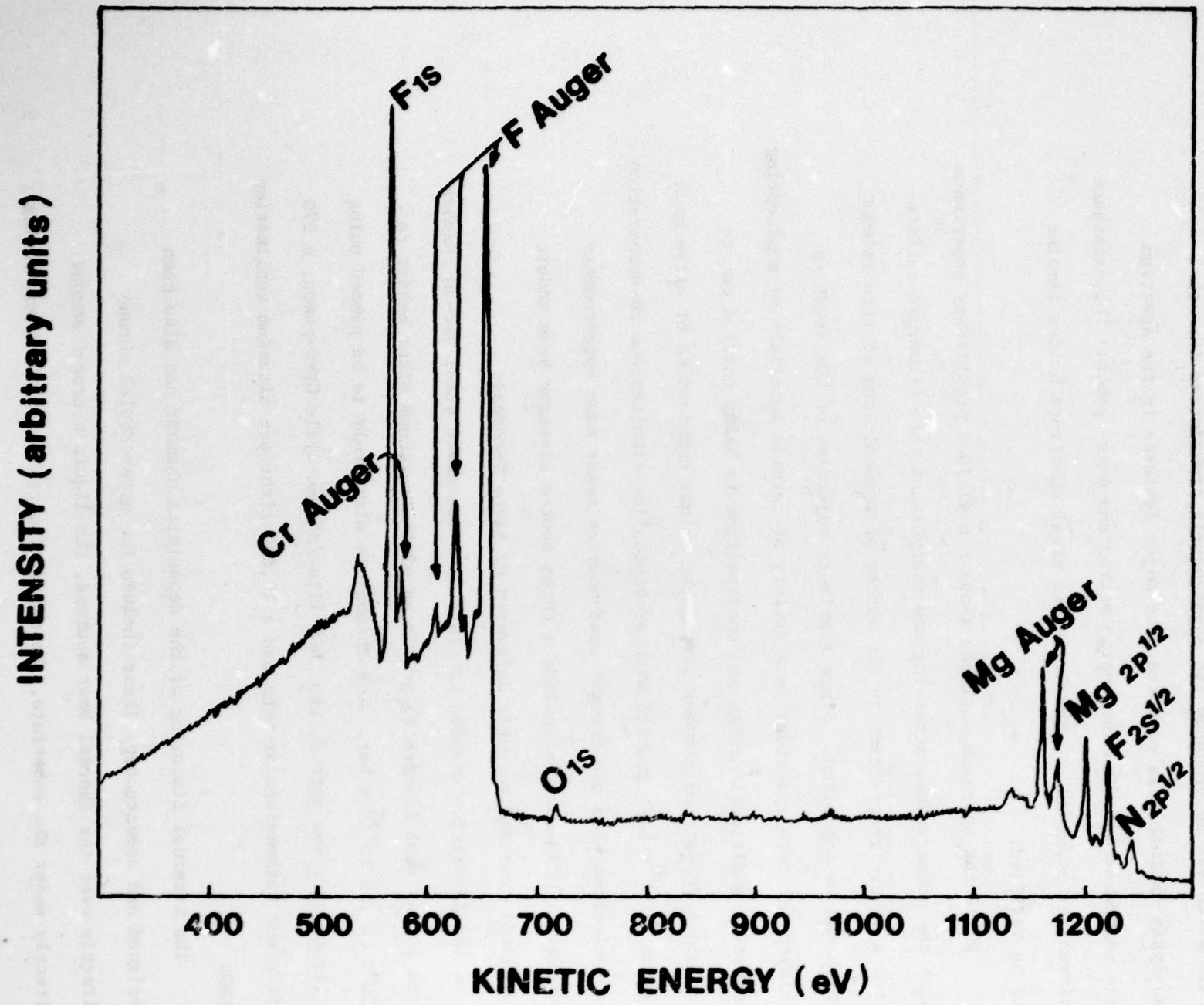

Figure 14. ESCA spectrum of MgF_2 film deposited on a Be-Cu substrate.

of the thickness of transparent antireflection films, a shutter wheel, a quartz crystal monitor, a mass spectrometer to monitor and supply a control signal for evaporation rates of the individual sources, and six thermal boat sources. Three transformers with silicon control rectifiers and process controllers have been constructed, and the process controllers to the microprocessor unit of the mass spectrometer have been connected to complete the circuit for servo control of the evaporation rate of individual sources.

The deposition subsystem should be completed with thermal boat evaporation and electron beam evaporation source capability in the very near future. At that time, the carousel load lock assembly should also be completed and should be connected to the deposition and analytical subsystems. It will then be possible to prepare thin films having a much wider range of compositions; in addition it will be possible to control the extent of crystallinity in a film by co-evaporating small amounts of glass forming impurities and by controlling the substrate temperatures.

Transfer of a specimen from the deposition chamber to the analytical subsystem will be accomplished using a 40" magnetic linear manipulator as pictured in Figure 12. A carousel type load-lock will be used in the final system to permit introduction of six substrate holding and stressing devices. As with the scheme using the Leybold Heraeus preparation chamber, stressing of the films will be accomplished by bending the substrate in the deposition system using the set screw of the stressable substrate holder.

A third approach involves the use of the entire system. Wire basket sources used in the Leybold preparation chamber are first coated with the ceramic composition of interest in the deposition chamber. These sources are then transfered to the Leybold preparation chamber; the substrate is introduced and sputter cleaned, and the coated wire basket is flash evaporated onto that substrate. The thin film-substrate combination is then analyzed as previously described. There are several advantages to this approach. Since the deposition chamber is only used for the preparation of the unique ceramic composition and not tied up for the analysis, there is a more efficient use of the facility. Also, since there is no need to fabricate a new stressing rig for the deposition chamber, results should be obtained more rapidly.

SUMMARY

Much of the effort during this past year has been devoted to the set up of a film deposition and surface analysis system to be used for the analysis of the effect of stress on chemical reactions. Preliminary results using Raman spectroscopy have suggested that there is an increase in the number of defects in the structure of fused silica under stress compared to the unstressed state. A model describing the effect of water diffusion controlled crack growth was discussed. It was shown that the presence of a relatively K_I independent region of crack growth has a significant effect on the proof testing of a material.

REFERENCES

1. S. M. Wiederhorn, "Influence of Water Vapor on Crack Propagation in Soda-Lime Glass", J. Am. Ceram. Soc. 50 407-14 (1967).
2. S. W. Freiman, "Effect of Alcohols on Crack Propagation in Glass", J. Am. Ceram. Soc. 57 350-53 (1974).
3. S. M. Wiederhorn and L. H. Bolz, "Stress Corrosion and Static Fatigue of Glass", J. Am. Ceram. Soc. 53 543-48 (1970).
4. D. P. H. Hasselman, pp 297-315 in Ultrafine-Grain Ceramics, ed. by J. J. Burke, N. L. Reed, and V. Weiss, Syracuse University Press, Syracuse, N.Y. (1970).
5. R. N. Stevens and R. Dutton, "Propagation of Griffith Cracks at High Temperature by Mass-Transport Processes," Mater. Sci. Eng. 8, 220-34 (1971).
6. W. W. Gerberich and M. Stout, "Discussion of Thermally Activated Approaches to Glass Fracture, J. Am. Ceram. Soc. 58, 222-225 (1976).
7. S. M. Cox, "Glass Strength and Ion Mobility", Phys. and Chem. Glasses, 10 226-39 (1969).
8. W. B. Hillig and R. J. Charles; pp 687-705 in High Strength Materials, edited by V. F. Zackary, John Wiley and Sons Inc., N.Y., 1965.
9. V. A. Bershtein, Yu. N. Mouchan and V. V. Nikitin, "Influence of Mechanical Stresses on the Hydrolysis of Bonds on the Surface of Glass," Soviet Physics Solid State 14 2422-23 (1973).
10. S. M. Wiederhorn, H. Johnson, A. M. Diness and A. H. Heuer, "Fracture of Glass in Vacuum:, J. Am. Ceram. Soc. 57, 336-41 (1974).
11. R. Buckner, Hans-Ulrich Chun, and H. Goretzki, Glastechn. Ber., 51, 1-7, (1978).
12. R. H. Stolen and G. E. Walrafen, "Water and Its Relation to Broken Bond Defects in Fused Silica," J. Chem. Phys., 64, 2623-30 (1976).
13. S. W. Freiman, "Effect of Straight-Chair Alkanes on Crack Propagation in Glass", J. Am. Ceram. Soc. 58, 339-40 (1975).